International Journal of Applied Glass Science

RESEARCH ARTICLE OPEN ACCESS

Zinc/Potassium-Doped Bioactive Glass With Enhanced Antimicrobial Activity Against Gram-Negative Bacteria

Devis Bellucci[1] | Francesco Basoli[2] | Simone De Micco[1] | Simone Grasso[3] | Marcella Trombetta[2] | Valeria Cannillo[1]

[1]Dipartimento di Ingegneria "Enzo Ferrari", Università di Modena e Reggio Emilia, Modena, Italy | [2]Dipartimento di Ingegneria, Università Campus Bio-Medico di Roma, Rome, Italy | [3]Dipartimento di Scienze e Bio-Tecnologie, Università Campus Bio-Medico di Roma, Rome, Italy

Correspondence: Valeria Cannillo (valeria.cannillo@unimore.it)

Received: 22 January 2026 | **Revised:** 5 March 2026 | **Accepted:** 10 April 2026

Keywords: antibacterial properties | bioactive glasses (BGs) | potassium doping | sintering | zinc doping

ABSTRACT

Bioactive glasses (BGs) are widely investigated for biomedical applications due to their bioactivity, ion release capability, and potential antimicrobial behavior. In this work, a novel zinc/potassium-doped BG, designated as Gaia-GN, was synthesized using the melt-quench technique. The thermal behavior was characterized through differential thermal analysis (DTA), thermogravimetry (TG), and heating microscopy (HM), which revealed a glass transition temperature of 513°C and a broad processing window suitable for viscous-flow sintering. Subsequently, Gaia-GN powders were thermally processed to obtain sintered specimens. XRD analysis showed that sintering at relatively low temperatures, namely 600°C, produced a compact and predominantly amorphous structure, minimizing the formation of crystalline phases. In addition, mechanical properties were evaluated by Vickers micro-indentation, determining Vickers hardness, Young's modulus, and fracture toughness using four different theoretical models. The results suggest that the combined presence of Zn and K improves thermal stability and mechanical performance compared with conventional formulations such as 45S5 Bioglass and S53P4. Finally, antimicrobial assays were conducted, revealing a strong antimicrobial action of the glass against Gram-negative bacteria. Overall, these findings underscore the potential of the new K/Zn-doped BG not only for its antibacterial properties but also for applications requiring thermal processing, such as the fabrication of scaffolds or coatings on metallic substrates.

1 | Introduction

Bioactive glasses (BGs) are a class of biomaterials known for their ability to bond to bone and soft tissues, stimulate repair processes, and release ions that drive specific biological responses. Since the development of 45S5 Bioglass by Hench in 1969 (mol%: 46.1 SiO_2, 26.9 CaO, 24.4 Na_2O, 2.6 P_2O_5), these materials have been extensively explored in orthopedics, dentistry, and tissue engineering [1]. The evolution of the field is commonly described in terms of three generations of biomaterials [2]. First-generation materials were designed simply to be inert and biocompatible. The discovery that 45S5 Bioglass could form a direct bond with bone initiated the second generation, characterized by bioactivity and controlled degradation. The subsequent emergence of third-generation biomaterials expanded this concept further, incorporating materials engineered at the molecular scale to modulate cellular behavior and actively promote tissue regeneration [1].

Although 45S5 is widely regarded as the archetype of second-generation biomaterials, certain BG compositions and processing methods enable properties typically associated with third-generation systems, especially when the materials are used in powder form or engineered for high reactivity. In particular, BGs can be tailored to provide functionalities such as antibacterial or angiogenic effects [3]. Two main strategies have been adopted to achieve antibacterial behavior [4]: doping the glass network

with therapeutic metal ions or designing rapidly dissolving compositions capable of inducing localized pH increases. Numerous studies have linked BG dissolution kinetics, pH elevation, and antimicrobial activity [5]. A prominent example is S53P4 (BonAlive; mol%: 53.8 SiO_2, 21.8 CaO, 22.7 Na_2O, 1.7 P_2O_5), the first BG reported to exhibit broad-spectrum antibacterial efficacy against both aerobic and anaerobic bacteria [6–8].

Among the various dopants introduced to enhance antibacterial activity, zinc (Zn) is one of the most extensively studied [9, 10]. Zn has been shown to promote osteoblast proliferation and differentiation, upregulate genes involved in angiogenesis and anti-inflammatory processes [11], reduce osteoclast function [12], increase alkaline phosphatase (ALP) production [11], and inhibit a broad spectrum of bacterial strains [13, 14]. Multiple mechanisms have been proposed for its bactericidal effect [15, 16], including interference with bacterial tolerance to acidic metabolites produced during glycolysis [17, 18], disruption of metal homeostasis, and induction of oxidative stress through reactive oxygen species formation [13, 16]. Structurally, ZnO primarily acts as a network modifier, reducing silicate network connectivity and increasing the amount of non-bridging oxygens, thereby enhancing the early dissolution rate and the release of Zn and Ca ions [19].

In addition to Zn, potassium (K) has been increasingly considered as an alternative network modifier in BG formulations [20–22]. K does not primarily act as an antibacterial ion; instead, its main role is related to structural and processing improvements [23, 24]. Several studies have demonstrated that partially or fully replacing Na_2O with K_2O reduces the crystallization tendency of melt-derived BGs, thereby improving their thermal stability during heat treatments such as sintering [24]. This effect has been associated with the ability of K^+ ions to alter glass network packing and shift the crystallization onset to higher temperatures [24]. For example, Arstila et al. reported that the addition of K_2O decreases the devitrification of typical Na/Ca–silicate BGs, enabling easier hot-working without undesirable phase formation [25]. Consistently, Cannillo et al. further confirmed that K-doped BGs inspired by 45S5 preserved thermomechanical properties and bioactivity while remaining amorphous after thermal processing, unlike 45S5, which partially crystallized during sintering [20]. Therefore, K-containing BGs represent an interesting class of compositions, particularly when manufacturing processes involve high temperatures, as they exhibit enhanced thermal stability.

These encouraging results underscore the need for investigation into new BG compositions containing Zn and K. Co-doped BGs containing both K and Zn have also been reported in the literature [26], although generally as part of multi-component formulations involving other modifiers [27, 28]. As a result, the simultaneous role of K and Zn in simpler silicate matrices has remained comparatively under-investigated.

In this work, we present a new glass composition designed to match the SiO_2 and P_2O_5 contents of the commercial S53P4 while providing a broader thermal processing window—defined as the temperature range between the glass transition temperature (T_G) and the onset of crystallization (T_{C_onset})—alongside lower sintering temperatures and higher crystallization temperatures. These features promote the preservation of an amorphous structure after sintering. The developed glass, designated as Gaia-GN, contains Zn and K and a reduced Na content compared with well-known silicate systems (e.g., 45S5 and S53P4). This tailored composition exhibits improved sinterability and marked antimicrobial activity against Gram-negative bacteria, positioning Gaia-GN as a promising candidate for further biomedical development.

2 | Materials and Methods

2.1 | Preparation of the BG Gaia-GN

Gaia-GN was synthesized via the melt-quench technique, following a procedure adopted for the preparation of similar materials [29]. The required amounts of finely powdered precursors (Carlo Erba Reagenti, Rodano-Milano, Italy) were weighed and mixed in a laboratory rotary mixer for 6 h to ensure a homogeneous mixture. The resulting batch was transferred into a platinum crucible and subjected to a controlled thermal treatment consisting of heating from room temperature to 1100°C at 10°C/min, followed by a decarbonation step at 1100°C for 1.5 h, subsequent heating to 1450°C at 10°C/min, and a final hold at 1450°C for 1 h to ensure a homogeneous melt. The melt was rapidly quenched in water to form a glass frit, which was dried at 110°C for 12 h, milled in a porcelain jar, and sieved to obtain powders with particle sizes below 63 μm. The nominal composition of the glass in mol% is: 53.8 SiO_2; 1.7 P_2O_5; 16.8 CaO; 12.7 Na_2O; 10 K_2O; 5 ZnO.

2.2 | Thermal Analyses

Thermal analyses were performed to characterize the behavior of Gaia-GN during heating. Differential thermal analysis (DTA) was carried out using the STA 429 CD system (Netzsch-Gerätebau GmbH, Selb, Germany). A total of 30 mg of powder was placed in a platinum crucible, and the temperature was increased from room temperature to 1200°C at a constant rate of 20°C/min. The resulting DTA curve allowed the identification of characteristic temperatures of the BG, including the glass transition temperature (T_G), the onset of crystallization temperature (T_{C_onset}), and the peak crystallization temperature (T_C).

Simultaneously, thermogravimetric (TG) measurements were performed to assess possible mass changes occurring upon heating. TG analysis was conducted under a dynamic air atmosphere (50 mL/min), and the resulting TG curve was used to determine the temperature intervals associated with mass loss. Furthermore, the thermal behavior of the glass powder at higher temperatures was investigated using a heating microscope (HM; Misura 3.32, Expert System Solutions, Modena, Italy). Samples were heated from room temperature to 1600°C at 10°C/min, allowing the determination of the sintering temperature (T_S) and melting temperature (T_M) of Gaia-GN.

2.3 | Sintering Behavior

To further investigate the influence of temperature on the sintering behavior, glass powders were compacted into disk-shaped

specimens and subjected to heat treatments at three selected temperatures: 580°C, 600°C, and 650°C. Sintering performance was evaluated by quantifying the extent of dimensional shrinkage ($\Delta_{\%}$), using the following equation [30]:

$$\Delta_{\%} = \frac{d_0 - d_s}{d_0} \times 100$$

where d_0 is the nominal diameter of the mold, and d_s is the diameter of the glass disk after sintering. The green bodies were produced by uniaxially pressing the powders at 7 bar for 10 s. For each formulation, the disk was placed in a muffle furnace (AWF 13/12, Lenton Laboratory & Scientific Equipment, Randburg, South Africa) and thermally treated at the designated temperatures using a heating rate of 5°C/min. After the thermal cycle, the specimens were allowed to cool to room temperature under ambient conditions. The final diameters were measured with a digital caliper (LTF 327.09, LTF S.p.A., Antegnate, Italy) to determine the shrinkage. The temperature at which the maximum reduction in size occurred was identified as the optimal sintering temperature (T_{BS}).

2.4 | Analysis of the Crystalline Phases

X-Ray diffraction (XRD) analysis was performed to investigate the eventual presence of crystalline phases formed in the samples subjected to different thermal treatments. The diffractometric analysis was conducted using an X'Pert PRO diffractometer (Panalytical, Almelo, the Netherlands) equipped with a Cu-Kα radiation source ($\lambda = 1.5406$ Å) operating at 40 kV and 40 mA. Data were collected in the 2θ range of 10°–70°, with a step size of 0.017°, in continuous scanning mode using a PIXcel3D detector.

2.5 | Study of Mechanical Properties: Hardness, Young's Modulus, and Fracture Toughness

The mechanical properties of the glass were evaluated on the sample sintered at 600°C for 1 h, which was selected based on the XRD results as the condition providing the optimal performance, using an Open Platform micro-indenter (CSM Instruments, Peseux, Switzerland) with a Vickers indenter tip. To determine the Vickers hardness and Young's modulus, indentations were performed under a maximum load of 0.5 N, with a loading/unloading rate of 1 N/min and a hold time of 15 s. At least 10 indentations were carried out, and the load-penetration depth curve was automatically recorded for each test. Young's modulus was calculated using the Oliver and Pharr method [31].

Fracture toughness was assessed using the same equipment by applying a load of 1 N, with a loading/unloading rate of 2 N/min and a hold time of 15 s. The values were calculated using four commonly applied theoretical methods [32–34] that relate the applied load (P) to the crack size generated by the Vickers indenter, assuming the formation of radial–median cracks, namely (i) Evans–Charles (EC), (ii) Lawn–Fuller (LF), (iii) Evans–Wilshaw (EW), and (iv) Lankford (L) [33, 34]:

i. EC model

$$K_{IC} = 0.0824 \cdot \left(P/c^{3/2}\right)$$

ii. LF model

$$K_{IC} = 0.0515 \cdot \left(P/c^{3/2}\right)$$

iii. EW model

$$K_{IC} = 0.079 \cdot \left(P/a^{3/2}\right) \cdot \log_{10} 4.5\,(a/c)$$

iv. L model

$$K_{IC} = 0.0363 \cdot (E/H_V)^{2/5} \cdot \left(P/a^{1.5}\right) \cdot (a/c)^{1.56}$$

where P is the applied load, c is the crack length measured from the center of the indent to the crack tip, a is the indentation half-diagonal length, E is the Young's modulus, and H_V is the Vickers hardness.

2.6 | Antimicrobial Study

To evaluate the antimicrobial activity of the BG powders, tests were conducted on both Gram-negative and Gram-positive bacterial strains. Freeze-dried *Escherichia coli* (Migula) Castellani and Chalmers (ATCC, Manassas, Virginia, USA), a Gram-negative bacterium, was revived by overnight incubation in Luria–Bertani (LB) medium at 37°C. To promote bacterial growth, 25 mL of liquid LB medium was added to enrich the culture. Similarly, freeze-dried *Staphylococcus aureus* (Seattle 1945) (ATCC, Manassas, Virginia, USA), a Gram-positive bacterium, was revived by overnight incubation in LB medium at 37°C and subsequently enriched by the addition of 25 mL of liquid LB medium.

Prior to testing, BG powders were placed in Petri dishes and sterilized under UV light for 3 h per side to ensure sterility. An extract was prepared by immersing the sterilized material in centrifuge tubes containing culture medium at a final concentration of 200 mg/mL, according to ISO 10993-12 guidelines [35]. The sample was incubated at 37°C for 72 h under gentle agitation to allow ion release. The resulting eluate was collected and used for subsequent antimicrobial assays.

Bacterial cultures were exposed to the BG-derived eluate, and the antimicrobial activity was evaluated by counting colony-forming units (CFUs) to determine bacterial growth inhibition. The plated concentrations were the same in both the controls and the treated plates. All experiments were performed in triplicate to ensure reproducibility and reliability of the results.

2.7 | Statistical Analysis

Statistical analyses were performed using Microsoft Excel (Microsoft Corporation, Redmond, WA, USA). Data are reported as mean values with their corresponding standard deviations (mean ± SD). All experiments were conducted in triplicate for each experimental condition. When appropriate, differences

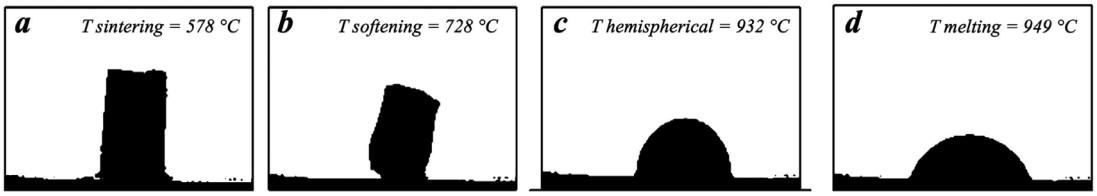

FIGURE 1 | HM analysis of the Gaia-GN sample.

TABLE 1 | Comparison of glass transition (T_G), crystallization onset (T_{C_onset}), crystallization (T_C), melting (T_M), and sintering (T_S) temperatures between 45S5 Bioglass [37], S53P4 [37], and the novel BG produced in this study.

	45S5 Bioglass	S53P4	Gaia-GN
Rate (°C/min)	20	20	20
T_G (°C)	520	530	513
T_{C_onset} (°C)	560	615	673
T_C (°C)	638	648	748
T_M (°C)	1193	1113	949
T_S (°C)	594	567	578
T_{BS} (°C)	1050	650	600
Processing window (°C)	40	85	160

between paired experimental conditions were evaluated using a one-tailed paired Student's *t*-test, with a significance level set at $p < 0.05$.

3 | Results and Discussion

3.1 | Thermal Analysis

The thermal behavior of the glass was assessed by HM, DTA, and TG. HM provides a sequence of geometrically analyzable images collected during heating, allowing the identification of the main characteristic temperatures [36] (Figure 1, and summarized in Table 1): (i) the sintering temperature (578°C); (ii) the softening temperature (728°C); (iii) the temperature for hemisphere formation (932°C); and (iv) the melting temperature (949°C). Compared with reference BGs—measured under the same heating rate (20°C/min)—the melting temperature of Gaia-GN is significantly lower than that of its parent glass S53P4 (1113°C), and 45S5 Bioglass (1193°C) [37]. This reduction reflects differences in network connectivity arising from Gaia-GN specific formulation, in which the reduced alkali content, the presence of potassium, and the specific balance between modifiers and intermediates result in a less rigid glass network requiring lower thermal energy to reach viscous flow [2, 38, 39]. In general terms, minor discrepancies in characteristic temperatures may also result from the granulometry used during thermal analysis, as this factor is known to influence thermal events [40]. For example, an increase in grain size is typically associated with higher crystallization temperatures [37, 40].

The DTA curve (Figure 2a) reveals a glass transition temperature (T_G) at 513°C and a higher crystallization onset and crystallization temperatures than both S53P4 and 45S5 Bioglass [37] (summarized in Table 1), while TG (Figure 2b) confirms that the material remains thermally stable over the investigated range, exhibiting only minor mass variations associated with the removal of surface-bonded volatiles. The reference values were measured by Bellucci et al. [37] under identical heating conditions and using powders with comparable granulometry. According to DTA, Gaia-GN begins crystallization above 673°C and reaches its crystallization peak at 748°C, offering a broader processing window (T_{C_onset}–T_G; Gaia-GN = 160°C) than 45S5 (processing window = 40°C) and S53P4 (processing window = 85°C). The reduced tendency to crystallize compared with commercial BGs can be presumably attributed to (i) Gaia-GN's lower Na_2O content, as sodium is known to promote crystallization [25]; (ii) the partial substitution of sodium with potassium [21], whose larger ionic radius increases structural distortion and consequently reduces the tendency to crystallize [2, 20, 21, 25, 37, 38, 41]; and (iii) the higher configurational entropy associated with the modified oxide composition, favoring amorphous retention [30]. Alkali oxides act as strong network modifiers, increasing non-bridging oxygens and lowering viscosity, thereby facilitating devitrification [25, 39, 42–44, 45]. In Gaia-GN, the reduced alkali content and the introduction of potassium and zinc mitigate this effect, and the enhanced stability is promising for applications requiring thermal treatments, such as scaffold fabrication or coatings [30].

It is important to note that these techniques primarily describe the onset of viscous flow and shrinkage, rather than effective densification or the achievement of mechanically compact materials. The DTA curve indicated a sintering window between 513°C (T_G) and 673°C (T_{C_onset}), suggesting that thermal treatments should be selected within this interval. HM measurements confirmed that viscous flow in Gaia-GN begins at temperatures higher than in S53P4 but significantly lower than in 45S5 Bioglass [46]. Furthermore, HM and DTA data revealed that Gaia-GN exhibits a sintering temperature higher than that of its parent glass S53P4, and lower than that of 45S5 Bioglass [37, 40]. This behavior represents a major advantage over 45S5 Bioglass, for which shrinkage and apparent sintering are often reported below 600°C, but true densification and mechanical integrity are typically achieved only after heat treatments exceeding 1000°C, as widely documented in the literature [44, 46, 47]. In contrast, Gaia-GN combines low-temperature densification with a wide processing window, enabling the production of compact amorphous components at temperatures below 700°C.

3.2 | Sintering Behavior

The degree of sintering was assessed by measuring the dimensional shrinkage before and after heat treatment at 600°C for

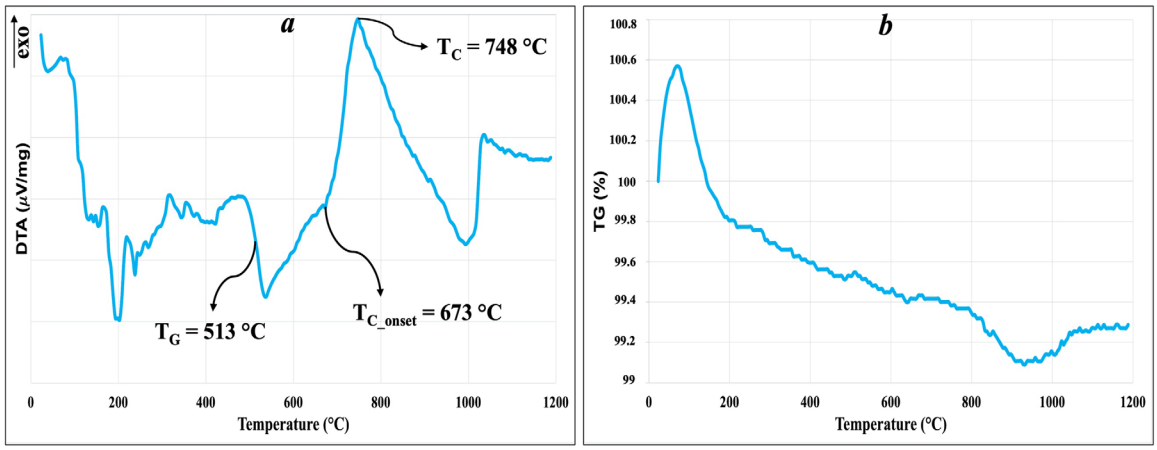

FIGURE 2 | DTA and TG analyses of Gaia-GN: (a) DTA—The characteristic temperatures T_G, T_{C_onset}, and T_C are shown on the curves. (b) TG.

1 h. This thermal treatment was specifically selected for the evaluation of sintering behavior because, as will be discussed in the following section, the samples treated in this way were found to be well sintered while remaining fully amorphous. For this reason, this condition was identified as the optimal compromise between effective densification and preservation of the amorphous structure.

A linear shrinkage of 14.0% ± 1.0% was obtained, indicating that a significant viscous-flow sintering process occurred at this temperature. Such a shrinkage level suggests effective particle rearrangement and pore closure, confirming that Gaia-GN reaches a viscosity suitable for densification without undergoing excessive deformation or structural instability [2, 48, 49]. However, compared with conventional BGs, this behavior appears markedly different [46, 50]. In the case of 45S5 Bioglass, sintering typically occurs through a multi-stage process, characterized by a limited initial densification at intermediate temperatures and a more pronounced shrinkage only at much higher temperatures [44, 46, 49]. The early stage, occurring around 650°C, is associated with minimal shrinkage, while significant densification is generally observed only above 900°C–1000°C [37, 44, 46, 49]. This behavior has been widely attributed to the early onset of crystallization, which restricts viscous flow and hinders effective densification at lower temperatures. The shrinkage associated with the first step measures ~2%, whereas a higher shrinkage rate of around 10% was recorded during the second phase [37]. On the other hand, S53P4 exhibits a comparatively improved sintering response, with shrinkage values in the range of 8–10% reported around 650°C, although the identification of an optimal sintering temperature remains debated, with different studies proposing temperatures from approximately 650°C to over 700°C [50–52]. These discrepancies further highlight the sensitivity of sintering behavior to the balance between viscous flow and the devitrification process.

In this framework, the pronounced shrinkage observed for Gaia-GN at 600°C can be attributed to (i) compositional modifications that favor an extended processing window between T_G and T_{C_onset} and (ii) the reduction of alkali content and the introduction of K and Zn, which are known to promote sintering by preserving an amorphous structure with adequate viscous mobility over a broader temperature range [9, 20, 23, 24]. This effect has been associated with multiple factors, including the reduced Na content, the low Na_2O/K_2O ratio, the stabilizing role of K_2O against devitrification [53], and the increased configurational entropy of the glass network. All of these factors contribute to suppressing crystallization at low temperatures and enabling efficient low-temperature densification [25, 53].

3.3 | Analysis of the Crystalline Phases

Figure 3 shows the XRD patterns of the samples treated at different temperatures: (a) 650°C for 3 h, (b) 600°C for 3 h, and (c) 600°C for 1 h. The diffractogram corresponding to the heat treatment at 650°C for 3 h reveals a clearer development of crystalline phases, indicating that higher temperature promotes partial crystallization of the glass matrix. In particular, the peaks suggested the formation of combeite ($Na_4Ca_4Si_6O_{18}$, JCPDS no. 01-079-1086). This aligns with previous studies on 45S5 Bioglass and S53P4 [37, 54, 55], which exhibit extremely narrow sintering windows, making thermal treatments particularly challenging due to the high risk of crystallization [2]. In BGs, sintering and crystallization are closely interconnected, often described as *sinter–crystallization* [56]. In many systems, crystallization may occur at early stages of thermal treatment, before sufficient viscous flow and densification are achieved, thereby limiting sintering efficiency [57]. The formation of crystalline phases reduces the available glassy phase for viscous flow, competing with densification and, in severe cases, leading to incomplete or heterogeneous shrinkage [58, 59].

Consistently, Gaia-GN treated at 600°C for 3 h displays a more amorphous character, with broader and less intense diffraction peaks, which probably may be related to the same crystalline phase ($Na_4Ca_4Si_6O_{18}$). By contrast, Gaia-GN treated at 600°C for 1 h preserves an amorphous character. Detecting crystallization is particularly relevant for BGs, as the development of crystalline phases may negatively affect their dissolution kinetics and bioactivity and may also lead to non-uniform degradation when implanted in vivo [37]. Gaia-GN exhibits a lower degree of crystallization compared to pure BGs [37], and, differently from other studies [24, 60], it does not show any peak associated with crystalline phases of K and/or Zn, which introduce distortions in the glass network, thereby impeding crystallization [2, 20, 38].

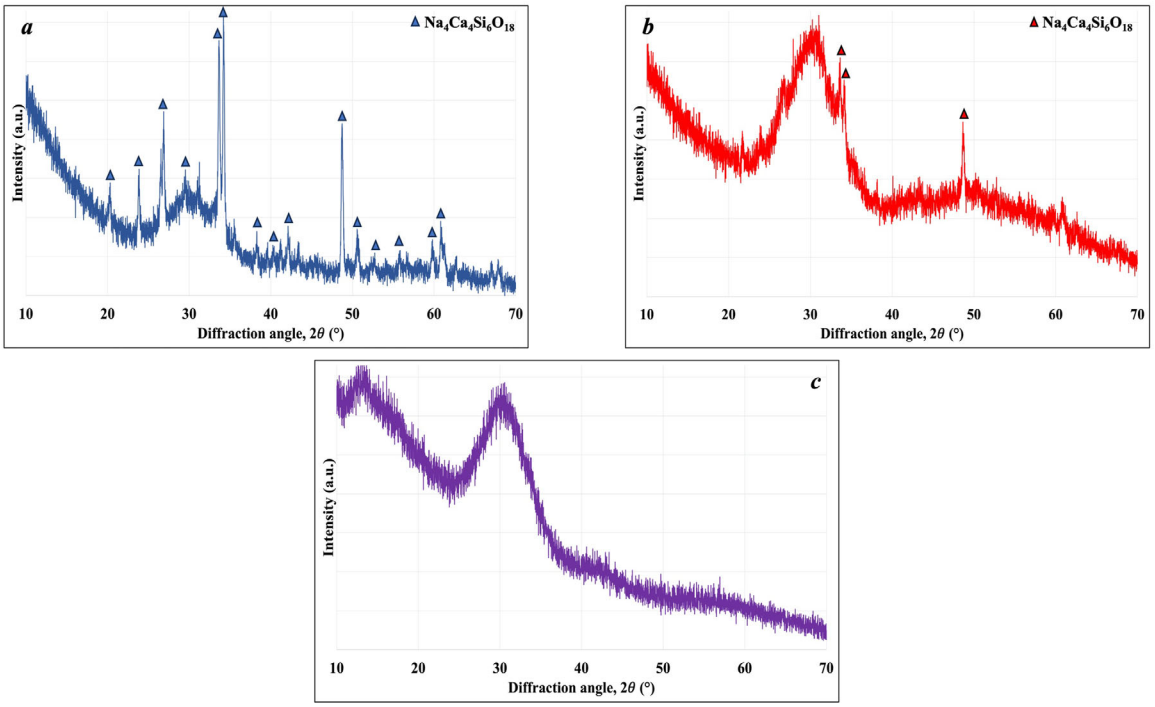

FIGURE 3 | XRD spectra of the sintered Gaia-GN: (a) 650°C for 3 h; (b) 600°C for 3 h; and (c) 600°C for 1 h.

TABLE 2 | Vickers hardness and Young's modulus (E_{IT}) measured at a maximum indentation load of 0.5 N, and fracture toughness (K_{IC}) measured at a maximum indentation load of 1 N, of the sintered Gaia-GN (600°C for 1 h) sample. EC, Evans–Charles; EW, Evans–Wilshaw; L, Lankford; LF, Lawn–Fuller.

Load 0.5 N		Load 1 N
H_V (GPa)	E_{IT} (GPa)	K_{IC} (MPa m$^{1/2}$)
6.99 ± 0.67	73.5 ± 3.1	0.77 ± 0.10 (EC)
		0.48 ± 0.06 (LF)
		0.73 ± 0.10 (EW)
		0.82 ± 0.11 (L)

In conclusion, for Gaia-GN, the combination of (i) substantial shrinkage and (ii) absence of crystalline peaks at 600°C for 1 h indicates that this temperature allows sintering to progress effectively before crystallization becomes significant.

3.4 | Mechanical Properties: Hardness, Young's Modulus, and Fracture Toughness

The mechanical behavior of Gaia-GN treated at 600°C for 1 h was determined via Vickers micro-indentation to assess hardness (H_V), indentation-derived Young's modulus (E_{IT}), and fracture toughness (K_{IC}). The H_V and E_{IT} were measured to be 6.99 ± 0.67 GPa and 73.5 ± 3.1 GPa, respectively, using a maximum indentation load of 0.5 N (Table 2). Under a higher indentation load of 1 N (Table 2), K_{IC} was calculated according to four classical models (EC, LF, EW, and L), yielding K_{IC} values in the range of 0.48–0.82 MPa · m$^{1/2}$ with average values around approximately 0.77 ± 0.10 MPa · m$^{1/2}$ (EC) and ~0.82 ± 0.11 MPa · m$^{1/2}$ (L).

Although a direct comparison is challenging due to differences in composition, processing, and testing methodologies, it is important to emphasize that our measurements were performed on samples sintered from powders, which may retain a certain level of residual porosity [61, 62]. It is well known that the porosity can negatively affect H_V, E_{IT}, and K_{IC} [61]. However, when compared with other sintered BG samples reported in the literature [30, 61, 63, 64], the relatively high H_V and E_{IT} values measured for Gaia-GN suggest a compact and rigid glass matrix, suitable for handling and potential shaping prior to biological testing. Furthermore, literature data on S53P4 [51, 55] and 45S5 indicate lower mechanical strength and K_{IC} values (on the order of ~0.6 MPa · m$^{1/2}$ for 45S5), which restrict their use mainly to non-load-bearing applications [65, 66].

On the other hand, doping BGs with metal ions (e.g., K^+, Zn^{2+}) may potentially improve mechanical performance by enhancing network rigidity, increasing cross-link density, or modifying bonding environments [23, 41, 67]. In particular: (i) in Zn-doped phosphate-based BG systems, increasing ZnO content within the investigated compositional range may lead to a progressive increase in both H_V and K_{IC} [67]; whereas, (ii) the addition of potassium oxide does not significantly affect the mechanical properties of the glass at comparable alkali contents, despite the lower field strength of K^+ relative to Na^+, suggesting that this substitution does not substantially modify the overall network connectivity [20]. Consistent with previous literature, these results indicate that zinc oxide plays a more significant role in enhancing the mechanical properties, contributing to the toughening of the glass–ceramic structure, whereas the effect of potassium oxide appears to be comparatively limited, with its

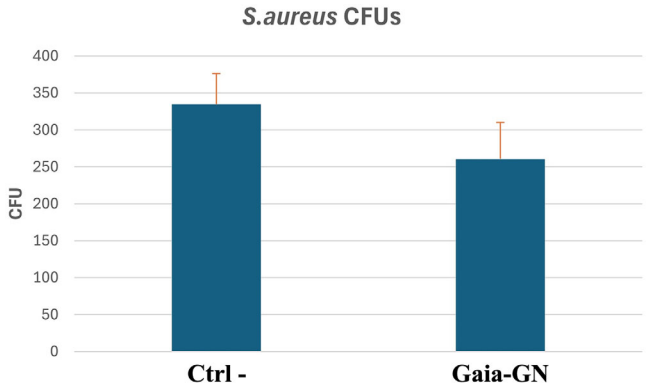

FIGURE 4 | CFU counts on both untreated (Ctrl) plates and Gaia-GN-treated plates against *S. aureus*. Error bars denote standard deviations from triplicate experiments.

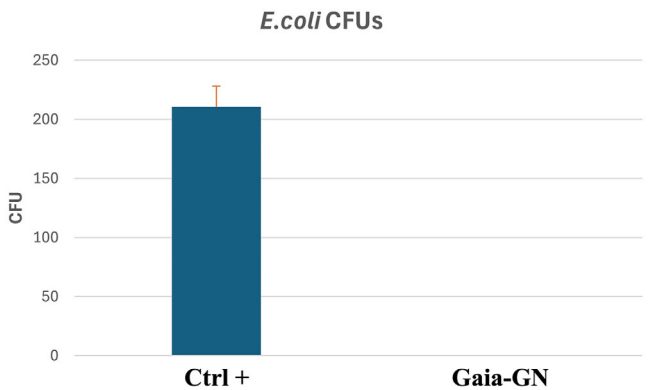

FIGURE 5 | CFU counts on both untreated (Ctrl) plates and Gaia-GN-treated plates against *E. coli*. Error bars denote standard deviations from triplicate experiments.

inclusion mainly justified by its favorable role in improving the thermal stability of the glass during thermal processing [20].

3.5 | Antibacterial Properties

The antimicrobial performance of Gaia-GN was tested both against *E. coli* and *S. aureus* by CFU counting. Figures 4 and 5 show the CFU counts on control (Ctrl) plates (untreated) and on plates treated with Gaia-GN, respectively, for *S. aureus* and *E. coli*. The plated bacterial concentrations were the same for both control and treated samples. Mean values and SD were calculated on three plates for each condition. Gaia-GN effectiveness against bacteria varied markedly between the two tested bacterial species. Against *E. coli*, Gaia-GN exhibited an impressive antimicrobial efficacy, achieving complete growth inhibition with a p-value < 0.05. In contrast, against *S. aureus*, the novel BG showed a much lower level of growth suppression. In this case, the statistical significance is slightly above the set threshold (p-value = 0.077).

These findings indicate that the tested BG formulation possesses physicochemical characteristics that result in a "double-face" behavior: excellent and consistent efficacy against Gram-negative bacteria, and a near-complete inefficacy (14% of antimicrobial efficiency) against Gram-positive bacteria (Figure 6). Further

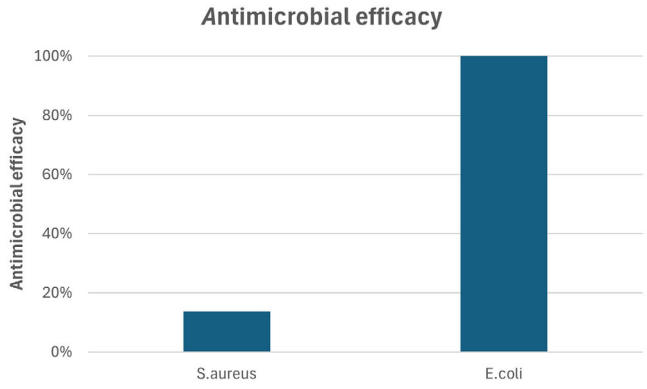

FIGURE 6 | Antimicrobial efficacy of Gaia-GN against *E. coli* and *S. aureus*. Efficacy was expressed as the percentage reduction in colony-forming units (CFUs) relative to untreated controls.

studies are warranted to elucidate the mechanistic basis of these differences, including nanoparticle–cell wall interactions, penetration efficiency, and stability under physiological conditions.

4 | Conclusions

A novel K/Zn-doped BG (Gaia-GN) was successfully synthesized and thermally processed. The melt-derived formulation exhibited a wide thermal processing window and enhanced thermal stability, promoted by the combined effect of K and Zn as network modifiers. HM and DTA confirmed the suitability of the material for viscous-flow sintering, whereas XRD analysis demonstrated that sintering at 600°C for 1 h maintained the glass in a largely amorphous state. The sintering process led to a significant degree of densification while preserving the shape and integrity of the specimens. Mechanical characterization revealed high H_V and good E_{IT} values, with a moderate K_{IC}, representing an improvement compared with conventional BGs such as 45S5 Bioglass and S53P4. In conclusion, antimicrobial assays revealed a strong inhibitory effect against *E. coli* (Gram-negative bacteria). Overall, Gaia-GN demonstrates promising thermomechanical properties and structural integrity after sintering, without compromising its amorphous nature, supporting its potential suitability for further development in antimicrobial and tissue engineering applications. Future investigations will focus on optimizing compositional parameters to further improve the performance of this class of BGs for bone repair, regenerative medicine, and antimicrobial activity, including against Gram-positive bacteria.

Acknowledgments

Funding for this research was provided under the National Recovery and Resilience Plan (NRRP), Mission 4, Component 2, Investment 1.1, Call for Tender No. 1409 published on September 14, 2022, by the Italian Ministry of University and Research (MUR), funded by the European Union–NextGenerationEU—Project Title: GAiA—Zero Waste Green Made Antimicrobial Filtering Face Piece Fibers for Augmented Individual Protection—CUP C53D23008340001—Grant Assignment Decree No. 966 adopted on June 30, 2023, by the MUR. Devis Bellucci and Valeria Cannillo wish to thank Dr. Francesco Gerardo Mecca and Dr. Andrea Martelli for their assistance during the sintering and the mechanical tests.

Open access publishing facilitated by Università degli Studi di Modena e Reggio Emilia, as part of the Wiley - CRUI-CARE agreement.

References

1. L. L. Hench, "The Story of Bioglass®," *Journal of Materials Science: Materials in Medicine* 17 (2006): 967–978, https://doi.org/10.1007/s10856-006-0432-z.

2. F. G. Mecca, D. Bellucci, and V. Cannillo, "Effect of Thermal Treatments and Ion Substitution on Sintering and Crystallization of Bioactive Glasses: A Review," *Materials* 16 (2023): 4651, https://doi.org/10.3390/ma16134651.

3. M. Godoy-Gallardo, U. Eckhard, L. M. Delgado, et al., "Antibacterial Approaches in Tissue Engineering Using Metal Ions and Nanoparticles: From Mechanisms to Applications," *Bioactive Materials* 6 (2021): 4470–4490, https://doi.org/10.1016/j.bioactmat.2021.04.033.

4. L. Drago, M. Toscano, and M. Bottagisio, "Recent Evidence on Bioactive Glass Antimicrobial and Antibiofilm Activity: A Mini-Review," *Materials* 11 (2018): 326, https://doi.org/10.3390/ma11020326.

5. S. Begum, W. E. Johnson, T. Worthington, and R. A. Martin, "The Influence of pH and Fluid Dynamics on the Antibacterial Efficacy of 45S5 Bioglass," *Biomedical Materials* 11 (2016): 015006, https://doi.org/10.1088/1748-6041/11/1/015006.

6. L. Hupa and N. C. Lindfors, "Bioactive Glass S53P4 – From a Statistically Suggested Composition to Clinical Success," in *Bioactive Glasses and Glass-Ceramics: Fundamentals and Applications*, ed. F. Baino and S. Kargozar (Wiley, 2022), 17–31, https://doi.org/10.1002/9781119724193.ch3.

7. O. Leppäranta, M. Vaahtio, T. Peltola, et al., "Antibacterial Effect of Bioactive Glasses on Clinically Important Anaerobic Bacteria In Vitro," *Journal of Materials Science: Materials in Medicine* 19 (2008): 547–551, https://doi.org/10.1007/s10856-007-3018-5.

8. E. Munukka, O. Leppäranta, M. Korkeamäki, et al., "Bactericidal Effects of Bioactive Glasses on Clinically Important Aerobic Bacteria," *Journal of Materials Science: Materials in Medicine* 19 (2008): 27–32, https://doi.org/10.1007/s10856-007-3143-1.

9. F. Sharifianjazi, M. Sharifianjazi, M. Irandoost, K. Tavamaishvili, M. Mohabatkhah, and M. Montazerian, "Advances in Zinc-Containing Bioactive Glasses: A Comprehensive Review," *Journal of Functional Biomaterials* 15 (2024): 258, https://doi.org/10.3390/jfb15090258.

10. I. Cacciotti, "Bivalent Cationic Ions Doped Bioactive Glasses: The Influence of Magnesium, Zinc, Strontium and Copper on the Physical and Biological Properties," *Journal of Materials Science* 52 (2017): 8812–8831, https://doi.org/10.1007/s10853-017-1010-0.

11. T. Tsuruoka, A. Kodama, S. Yamaguchi, et al., "Zinc Deficiency Impairs Ischemia-Induced Angiogenesis," *JVS-Vascular Science* 3 (2022): 30–40, https://doi.org/10.1016/j.jvssci.2021.09.023.

12. F. Rehder, M. Arango-Ospina, S. Decker, et al., "The Addition of Zinc to the ICIE16-Bioactive Glass Composition Enhances Osteogenic Differentiation and Matrix Formation of Human Bone Marrow-Derived Mesenchymal Stromal Cells," *Biomimetics* 9 (2024): 53, https://doi.org/10.3390/biomimetics9010053.

13. C. R. Mendes, G. Dilarri, C. F. Forsan, et al., "Antibacterial Action and Target Mechanisms of Zinc Oxide Nanoparticles Against Bacterial Pathogens," *Scientific Reports* 12 (2022): 2658, https://doi.org/10.1038/s41598-022-06657-y.

14. N. Pangprasit, A. Kongkaew, D. Saipinta, et al., "Evaluation of Antibacterial Properties of Zinc Oxide Nanoparticles Against Bacteria Isolated From Animal Wounds," *Pharmaceutics* 17 (2025): 209, https://doi.org/10.3390/pharmaceutics17020209.

15. T.-N. Phan, T. Buckner, J. Sheng, J. D. Baldeck, and R. E. Marquis, "Physiologic Actions of Zinc Related to Inhibition of Acid and Alkali Production by Oral Streptococci in Suspensions and Biofilms," *Oral Microbiology Immunology* 19 (2004): 31–38, https://doi.org/10.1046/j.0902-0055.2003.00109.x.

16. V. K. H. Bui, D. Park, and Y. C. Lee, "Chitosan Combined With ZnO, TiO_2 and Ag Nanoparticles for Antimicrobial Wound Healing Applications: A Mini Review of the Research Trends," *Polymers* 9 (2017): 21, https://doi.org/10.3390/polym9010021.

17. V. Anand, K. J. Singh, and K. Kaur, "Evaluation of Zinc and Magnesium Doped 45S5 Mesoporous Bioactive Glass System for the Growth of Hydroxyl Apatite Layer," *Journal of Non-Crystalline Solids* 406 (2014): 88–94, https://doi.org/10.1016/j.jnoncrysol.2014.09.050.

18. M. M. Almoudi, A. S. Hussein, M. I. Abu Hassan, and N. Mohamad Zain, "A Systematic Review on Antibacterial Activity of Zinc Against *Streptococcus mutans*," *Saudi Dental Journal* 30 (2018): 283–291, https://doi.org/10.1016/j.sdentj.2018.06.003.

19. N. Kanzaki, K. Onuma, G. Treboux, S. Tsutsumi, and A. Ito, "Inhibitory Effect of Magnesium and Zinc on Crystallization Kinetics of Hydroxyapatite (0001) Face," *Journal of Physical Chemistry B* 104 (2000): 4189–4194, https://doi.org/10.1021/jp9939726.

20. V. Cannillo and A. Sola, "Potassium-Based Composition for a Bioactive Glass," *Ceramics International* 35 (2009): 3389–3393, https://doi.org/10.1016/j.ceramint.2009.06.011.

21. M. Brink, "The Influence of Alkali and Alkaline Earths on the Working Range for Bioactive Glasses," *Journal of Biomedical Materials Research* 36 (1997): 109–117, https://doi.org/10.1002/(SICI)1097-4636(199707)36:1%3c109::AID-JBM13%3e3.0.CO;2-D.

22. M. Shoaib, A. Saeed, J. Akhtar, et al., "Potassium-Doped Mesoporous Bioactive Glass: Synthesis, Characterization and Evaluation of Biomedical Properties," *Materials Science and Engineering C* 75 (2017): 836–844, https://doi.org/10.1016/j.msec.2017.02.090.

23. D. Bellucci, V. Cannillo, and A. Sola, "Calcium and Potassium Addition to Facilitate the Sintering of Bioactive Glasses," *Materials Letters* 65 (2011): 1825–1827, https://doi.org/10.1016/j.matlet.2011.03.060.

24. D. Bellucci, V. Cannillo, and A. Sola, "A New Potassium-Based Bioactive Glass: Sintering Behaviour and Possible Applications for Bioceramic Scaffolds," *Ceramics International* 37 (2011): 145–157, https://doi.org/10.1016/j.ceramint.2010.08.020.

25. H. Arstila, L. Hupa, K. H. Karlsson, and M. Hupa, "Influence of Heat Treatment on Crystallization of Bioactive Glasses," *Journal of Non-Crystalline Solids* 354 (2008): 722–728, https://doi.org/10.1016/j.jnoncrysol.2007.06.092.

26. X. Chen, D. S. Brauer, N. Karpukhina, et al., "'Smart' Acid-Degradable Zinc-Releasing Silicate Glasses," *Materials Letters* 126 (2014): 278–280, https://doi.org/10.1016/j.matlet.2014.04.009.

27. P. Balasubramanian, L. A. Strobel, U. Kneser, and A. R. Boccaccini, "Zinc-Containing Bioactive Glasses for Bone Regeneration, Dental and Orthopedic Applications," *Biomedical Glasses* 1 (2015): 51–69, https://doi.org/10.1515/bglass-2015-0006.

28. V. Mosquim, D. G. Gillam, L. Wang, and R. G. Hill, "Multi-Component SiO_2–P_2O_5–Na_2O–K_2O–CaO–SrO–ZnO–CaF_2–SrF_2 Bioactive Glass With a Lower Fluoride Content Can Form Strontium-Containing Fluorapatite: A 19 F MAS-NMR Analysis," *Journal of Materials Chemistry B* 13 (2025): 13725–13736, https://doi.org/10.1039/d5tb00060b.

29. D. Bellucci and V. Cannillo, "Low-Temperature Sintering of a New Bioactive Glass Enriched With Magnesium Oxide and Strontium Oxide," *Materials* 15 (2022): 6263, https://doi.org/10.3390/ma15186263.

30. A. Martelli, D. Bellucci, and V. Cannillo, "An Enhanced Bioactive Glass Composition With Improved Thermal Stability and Sinterability," *Materials* 17 (2024): 6175, https://doi.org/10.3390/ma17246175.

31. W. C. Oliver and G. M. Pharr, "An Improved Technique for Determining Hardness and Elastic Modulus Using Load and Displacement Sensing Indentation Experiments," *Journal of Materials Research* 7 (1992): 1564–1583, https://doi.org/10.1557/jmr.1992.1564.

32. M. Sakai and R. C. Bradt, "Fracture Toughness Testing of Brittle Materials," *International Materials Reviews* 38 (1993): 53–78, https://doi.org/10.1179/imr.1993.38.2.53.

33. C. B. Ponton and R. D. Rawlings, "Vickers Indentation Fracture Toughness Test Part 1 Review of Literature and Formulation of Standardised Indentation Toughness Equations," *Materials Science and Technology* 5 (1989): 865–872, https://doi.org/10.1179/mst.1989.5.9.865.

34. C. B. Ponton and R. D. Rawlings, "Vickers Indentation Fracture Toughness Test Part 2 Application and Critical Evaluation of Standardised Indentation Toughness Equations," *Materials Science and Technology* 5 (1989): 961–976, https://doi.org/10.1179/mst.1989.5.10.961.

35. International Standard ISO 10993-12, *Biological Evaluation of Medical Devices—Part 12: Sample Preparation and Reference Materials*, ISO 10993-12:2012(E) (ISO, 2012), https://www.iso.org.

36. C. Venturelli, "Heating Microscopy and Its Applications," *Microscopy Today* 19 (2011): 20–25, https://doi.org/10.1017/s1551929510001185.

37. D. Bellucci, A. Mazzilli, A. Martelli, et al., "Enrichment of Strontium and Magnesium Improves the Physical, Mechanical and Biological Properties of Bioactive Glasses Undergoing Thermal Treatments: New Cues for Biomedical Applications," *Ceramics International* 50 (2024): 52819–52837, https://doi.org/10.1016/j.ceramint.2024.10.135.

38. A. Marikani, A. Maheswaran, M. Premanathan, and L. Amalraj, "Synthesis and Characterization of Calcium Phosphate Based Bioactive Quaternary P_2O_5–CaO–Na_2O–K_2O Glasses," *Journal of Non-Crystalline Solids* 354 (2008): 3929–3934, https://doi.org/10.1016/j.jnoncrysol.2008.05.005.

39. I. L. Denry and J. A. Holloway, "Effect of Sodium Content on the Crystallization Behavior of Fluoramphibole Glass-Ceramics," *Journal of Biomedical Materials Research* 63 (2002): 48–52, https://doi.org/10.1002/jbm.10085.

40. J. Massera, S. Fagerlund, L. Hupa, and M. Hupa, "Crystallization Mechanism of the Bioactive Glasses, 45S5 and S53P4," *Journal of the American Ceramic Society* 95 (2012): 607–613, https://doi.org/10.1111/j.1551-2916.2011.05012.x.

41. C. B. Cevlik, A. C. Ozarslan, B. Karakuzu Ikizler, Y. B. Elalmis, and S. Yücel, "Investigation of Mg, K, Cu, Zn Doped S53P4 Bioactive Glass In Vitro Studies; Bioactivity and Biodegradability Features," *Journal of the Indian Chemical Society* 96 (2019): 1131–1136.

42. F. Branda, A. Costantini, G. Luciani, and G. Laudisio, "The Role of Trivalent Element Oxides in CaO (Na_2O)–M_2O_3–SiO_2 Glasses From Tg," *Journal of Thermal Analysis and Calorimetry* 64 (2001): 1017–1024, https://doi.org/10.1023/A:1011595618322.

43. J. Jiusti, E. D. Zanotto, S. A. Feller, et al., "Effect of Network Formers and Modifiers on the Crystallization Resistance of Oxide Glasses," *Journal of Non-Crystalline Solids* 550 (2020): 120359, https://doi.org/10.1016/j.jnoncrysol.2020.120359.

44. O. Bretcanu, X. Chatzistavrou, K. Paraskevopoulos, R. Conradt, I. Thompson, and A. R. Boccaccini, "Sintering and Crystallisation of 45S5 Bioglass® Powder," *Journal of the European Ceramic Society* 29 (2009): 3299–3306, https://doi.org/10.1016/j.jeurceramsoc.2009.06.035.

45. G. S. Lázaro, S. C. Santos, C. X. Resende, and E. A. dos Santos, "Individual and Combined Effects of the Elements Zn, Mg and Sr on the Surface Reactivity of a SiO_2·CaO·Na_2O·P_2O_5 Bioglass System," *Journal of Non-Crystalline Solids* 386 (2014): 19–28, https://doi.org/10.1016/j.jnoncrysol.2013.11.038.

46. Q. Z. Chen, I. D. Thompson, and A. R. Boccaccini, "45S5 Bioglass®-Derived Glass-Ceramic Scaffolds for Bone Tissue Engineering," *Biomaterials* 27 (2006): 2414–2425, https://doi.org/10.1016/j.biomaterials.2005.11.025.

47. R. Wetzel, M. Blochberger, F. Scheffler, L. Hupa, and D. S. Brauer, "Mg or Zn for Ca Substitution Improves the Sintering of Bioglass 45S5," *Scientific Reports* 10 (2020): 15964, https://doi.org/10.1038/s41598-020-72091-7.

48. A. Mari, M. Pavarini, P. F. Menci, C. Charbonneau, L. P. Lefebvre, and L. De Nardo, "Impact of Aging on the Sintering Behavior of Bioactive-Glass Powder," *Journal of Materials Research and Technology* 25 (2023): 3704–3711, https://doi.org/10.1016/j.jmrt.2023.06.204.

49. L. Lefebvre, L. Gremillard, J. Chevalier, R. Zenati, and D. Bernache-Assolant, "Sintering Behaviour of 45S5 Bioactive Glass," *Acta Biomaterialia* 4 (2008): 1894–1903, https://doi.org/10.1016/j.actbio.2008.05.019.

50. G. Strömberg, L. Aalto-Setälä, P. Uppstu, et al., "Development and Characterization of Non-Coated and PLGA-Coated S53P4 and S59 Bioactive Glass Scaffolds for Treatment of Load-Bearing Defects," *Biomedical Materials and Devices* 2 (2024): 498–509, https://doi.org/10.1007/s44174-023-00099-4.

51. S. Fagerlund, J. Massera, N. Moritz, L. Hupa, and M. Hupa, "Phase Composition and In Vitro Bioactivity of Porous Implants Made of Bioactive Glass S53P4," *Acta Biomaterialia* 8 (2012): 2331–2339, https://doi.org/10.1016/j.actbio.2012.03.011.

52. C. M. E. Rustenburg, J. W. Snuggs, K. S. Emanuel, et al., "Modelling the Catabolic Environment of the Moderately Degenerated Disc With a Caprine Ex Vivo Loaded Disc Culture System," *European Cells & Materials* 40 (2020): 21–37, https://doi.org/10.22203/eCM.v040a02.

53. E. Verné, O. Bretcanu, C. Balagna, et al., "Early Stage Reactivity and In Vitro Behavior of Silica-Based Bioactive Glasses and Glass-Ceramics," *Journal of Materials Science: Materials in Medicine* 20 (2009): 75–87, https://doi.org/10.1007/s10856-008-3537-8.

54. C. Berbecaru, H. V. Alexandru, G. E. Stan, D. A. Marcov, I. Pasuk, and A. Ianculescu, "First Stages of Bioactivity of Glass-Ceramics Thin Films Prepared by Magnetron Sputtering Technique," *Materials Science and Engineering: B* 169 (2010): 101–105, https://doi.org/10.1016/j.mseb.2010.01.007.

55. A. Stiller, M. Engblom, E. Vainio, and L. Hupa, "Understanding the Crystallization Behavior of Bioactive Glass S53P4 Powder Compacts Under Various Heating Conditions," *Journal of Non-Crystalline Solids* 644 (2024): 123178, https://doi.org/10.1016/j.jnoncrysol.2024.123178.

56. F. Baino and E. Fiume, "Mechanical Characterization of 45S5 Bioactive Glass-Derived Scaffolds," *Materials Letters* 245 (2019): 14–17, https://doi.org/10.1016/j.matlet.2019.02.086.

57. A. R. Boccaccini, Q. Chen, L. Lefebvre, L. Gremillard, and J. Chevalier, "Sintering, Crystallisation and Biodegradation Behaviour of Bioglass®-Derived Glass-Ceramics," *Faraday Discussions* 136 (2007): 27–44, https://doi.org/10.1039/b616539g.

58. L. Lin, L. Zhang, J. Wang, et al., "Low-Temperature Sintering of 45S5 Bioglass®-Based Glass Ceramics: Effect of Biphasic Mixing Approach on the Mechanical and Biological Properties," *Materials Letters* 126 (2014): 154–158, https://doi.org/10.1016/j.matlet.2014.04.028.

59. C. Blaeß, R. Müller, G. Poologasundarampillai, and D. S. Brauer, "Sintering and Concomitant Crystallization of Bioactive Glasses," *International Journal of Applied Glass Science* 10 (2019): 449–462, https://doi.org/10.1111/ijag.13477.

60. Z. Y. Wu, R. G. Hill, S. Yue, D. Nightingale, P. D. Lee, and J. R. Jones, "Melt-Derived Bioactive Glass Scaffolds Produced by a Gel-Cast Foaming Technique," *Acta Biomaterialia* 7 (2011): 1807–1816, https://doi.org/10.1016/j.actbio.2010.11.041.

61. D. Bellucci, A. Sola, and V. Cannillo, "Bioactive Glass-Based Composites for the Production of Dense Sintered Bodies and Porous Scaffolds," *Materials Science and Engineering C* 33 (2013): 2138–2151, https://doi.org/10.1016/j.msec.2013.01.029.

62. J. Liu, H. Hu, P. Li, C. Shuai, and S. Peng, "Fabrication and Characterization of Porous 45S5 Glass Scaffolds via Direct Selective Laser Sintering," *Materials and Manufacturing Processes* 28 (2013): 610–615, https://doi.org/10.1080/10426914.2012.736656.

63. Z. W. Loh, M. H. Mohd Zaid, K. A. Matori, et al., "Phase Transformation and Mechanical Properties of New Bioactive Glass-Ceramics Derived From CaO–P_2O_5–Na_2O–B_2O_3–SiO_2 Glass System," *Journal of the Mechanical Behavior of Biomedical Materials* 143 (2023): 105889, https://doi.org/10.1016/j.jmbbm.2023.105889.

64. A. Mabrouk, A. Bachar, A. Atbir, et al., "Mechanical Properties, Structure, Bioactivity and Cytotoxicity of Bioactive Na-Ca-Si-P-O-(N)

Glasses," *Journal of the Mechanical Behavior of Biomedical Materials* 86 (2018): 284–293, https://doi.org/10.1016/j.jmbbm.2018.06.023.

65. G. Kaur, V. Kumar, F. Baino, et al., "Mechanical Properties of Bioactive Glasses, Ceramics, Glass-Ceramics and Composites: State-of-the-Art Review and Future Challenges," *Materials Science and Engineering C* 104 (2019): 109895, https://doi.org/10.1016/j.msec.2019.109895.

66. N. Al-Harbi, H. Mohammed, Y. Al-Hadeethi, et al., "Silica-Based Bioactive Glasses and Their Applications in Hard Tissue Regeneration: A Review," *Pharmaceuticals* 14 (2021): 75, https://doi.org/10.3390/ph14020075.

67. M. Mohan Babu, P. Syam Prasad, S. Hima Bindu, et al., "Investigations on Physico-Mechanical and Spectral Studies of Zn^{2+} Doped P_2O_5-Based Bioglass System," *Journal of Composites Science* 4 (2020): 129, https://doi.org/10.3390/jcs4030129.